IEEE Access
Multidisciplinary | Rapid Review | Open Access Journal

Received July 3, 2020, accepted July 15, 2020, date of publication July 27, 2020, date of current version August 7, 2020.

Digital Object Identifier 10.1109/ACCESS.2020.3012031

Design of a Variable Stiffness Joint Module to Quickly Change the Stiffness and to Reduce the Power Consumption

NAGAMANIKANDAN GOVINDAN[1], SHASHANK RAMESH[2], AND ASOKAN THONDIYATH[1], (Senior Member, IEEE)

[1]Department of Engineering Design, Indian Institute of Technology Madras, Chennai 600036, India
[2]Department of Mechanical Engineering, Indian Institute of Technology Madras, Chennai 600036, India

Corresponding author: Nagamanikandan Govindan (nagamani.gi@ gmail.com)

ABSTRACT Variable stiffness actuators (VSA) are finding wide applications in robotics to enhance safety during interactions with stiff environments. Researchers have proposed various design architectures like antagonistic actuation, which requires both the motors to be powered simultaneously for varying the stiffness or equilibrium position. In this paper, the design of a novel joint module, named as variable stiffness joint module (VSJM), is proposed, which consists of a lead-screw arrangement for varying the stiffness range and a cam based mechanism to change the stiffness within the set range quickly. The cam profile has been synthesized to maximize the stiffness variation as well as to maintain the cam and cam follower in static equilibrium when the output link is in the equilibrium position. This was achieved by properly positioning and orienting the friction cones at the contact points. By mechanically compensating the moment due to unbalanced forces at the contact points, the continuous usage of stiffness motor has been eliminated, leading to reduced power consumption. Details of the proposed mechanism are presented along with the mathematical model for cam profile synthesis and static analysis. A simplified prototype of the proposed design has been fabricated to perform the experiments. A hammering-a-nail experiment has been conducted to show the capability of the mechanism, and the results are presented.

INDEX TERMS Variable stiffness actuator, flexible joint, cam mechanism, static equilibrium.

I. INTRODUCTION

A robotic system made of rigid links to collaborate or interact with an external agent or environment must have an adjustable elasticity, at least at the joint level. Controlling the joint elasticity is crucial [1], to reduce the mechanical damages and to ensure system stability. This was addressed in the literature by providing active or passive compliance control [2], [3], which would change the elasticity of the joint, based on the task requirement. The active methods need force/torque sensors or torque-controlled motors, which are highly expensive, and the motors are generally regulated through software programming. Even though active methods are accurate, rigid impacts or delayed response due to processing of sensory inputs would damage the joint motors. To overcome this problem, passive compliance control, which incorporates a passive element such as a spring or elastic material is preferred in many situations [4] like grasping, walking, and manufacturing operations like drilling, hammering, and grinding.

The presence of a passive element in the joint decouples the actuator and the link from the external disturbances. However, finding a proper value for the joint stiffness is critical, as increasing the joint stiffness makes the system more sensitive to external disturbances. On the other hand, decreasing joint stiffness makes the system sloppy and may lead to undesired oscillations. Therefore, the joint module should have the ability to change the stiffness of the passive element. Variable stiffness actuators that are equipped with a dedicated actuator to vary the characteristics of passive elastic elements to change the joint stiffness are generally employed in such situations.

In general, VSA with a passive element can be implemented through different actuation methods, namely,

The associate editor coordinating the review of this manuscript and approving it for publication was Giambattista Gruosso.

antagonistic motor and independent motor setup, as described in [5]. In combination with the actuation method, different stiffness variation method, such as, changing the pretension of the passive element, changing transmission between load and spring (CompAct-VSA [6], AwAS [7], AwAS II [8], vsaUT II [9]), and changing physical properties of the elastic elements (like flexible elements [10], [11] and McKibben [12], [13]) have been employed in the prior art. Some of the notable designs, such as antagonistic springs with antagonistic motors (VSA-II [14], BAVS [15]), antagonistic springs with independent motors (AMASC [16], [17] and [18]), and independent motor for changing the stiffness and equilibrium position (Maccepa [19], Maccepa 2.0 [20], DLR FSJ [21], SVSA [22]) can also be found in the literature. More information about various designs, classifications, and characteristics of VSA can be found in the review articles [5], [23]–[25]. Usually, variable stiffness joints consist of two actuators that have to be powered continuously for changing the joint angle and joint stiffness. For instance, though the antagonistic method has the advantage of reduced inertia due to indirect actuation, the motors should act against each other to change the stiffness or equilibrium position. Therefore, the change in equilibrium position and stiffness are coupled. As a result, the mechanical power remains zero (in the equilibrium position) for the nonzero electrical power since the motor has to provide the torque continuously to maintain the stiffness. As a consequence, the motors consume power, even if the output motion is absent, which is a significant drawback of antagonistic methods.

Vanderborght *et al.* [26] and Chalvet and Braun [27] have compared and quantified the energy consumption of different variable stiffness designs and shown the significance. In addition to that, Verstraten *et al.* [28] have compared the energy consumption of series elastic actuators (SEA) and parallel elastic actuators (PEA). Apart from comparing different designs, a few methods can be found in the literature [7], [29]–[32], where reducing power consumption has been considered as a design requirement. Of them, designs like MeRIA [31], [32] and AwAS [7], used lead screws, which allow the mechanism to maintain the stiffness without dissipating the power due to non-back drivability characteristics. However, the change in stiffness would not be instantaneous due to the lead screw arrangement. Particularly in some cases, the system should instantaneously change the stiffness to absorb the energy during the contact with the environment, or to inject energy into the system in other cases. Further, decoupling the control of stiffness and the position can be achieved by coupling the endpoints of the springs either through lever arm mechanism [7]–[9], [30], [33], [34], or cam mechanism [15], [34], [35]. Also, implementing a lever arm mechanism for varying the stiffness by changing the transmission ratio between the internal elastic element and the motor would affect the compactness. In some designs, an extra electromechanical component like a clutch or brake is used to engage elastic elements that are arranged in series or parallel to vary the stiffness discretely [36]–[38]. The additional on-off devices for recruiting the elastic elements would result in increased power consumption and complexity of the system. It also requires a specific activation pattern to vary the predefined available stiffness values. The discontinuous changes in stiffness during the operation of the discrete variable stiffness actuators may result in a transient impulsive force at the output link, which is undesired, mainly when the joint is used in collaborative robots. Generally, the high output torque requirement is achieved at the cost of compromising the compactness, as in the case of Maccepa [19] due to single spring usage. The compactness is directly affected by the size of the elastic element.

Though various VSA designs have been implemented successfully, there remains a need to develop a compact, versatile joint module that utilizes less power and quickly changes the stiffness. In most cases, the consumption of power is mainly reduced by minimizing the cause of energy dissipation (i.e., friction associated with the transmissions and spring elements), and less importance has been given to reduce the power consumption further at the design level. Also, most of the available VSA designs are capable of changing the stiffness, but the range of stiffness of such designs remains fixed. In order to achieve lower joint impedance, the length of the spring has to be increased, which directly affects the compactness of the mechanism. To address these issues, a new design has been proposed in this paper to change the stiffness in two different ways: 1) modify the range of the stiffness using lead-screw arrangement 2) vary the stiffness within each range using a cam mechanism. In addition to that, the equilibrium position of the output link could be maintained without actuating the stiffness motor, leading to reduced power dissipation. The proposed joint module suits applications such as human-robot interactions, rehabilitation purposes, and explosive movements.

The remainder of this paper is organized as follows: In Section II, we present the design concept of the proposed VSJM. Subsequently, the working principle, detailed synthesis and analysis, and design procedures are described in Section III. Following that, in Section IV, the static analysis and stiffness modeling will be presented. Section V provides detailed CAD modeling, spring design, and construction of the VSJM. In Section VI, we discuss the experimental results and present an algorithm for the hammering task to show the application potential of the joint module.

II. DESIGN CONCEPT

The simplified architecture of the VSJM module comprises of variable stiffness mechanism (VSM), input and output link to connect with the adjacent joint modules, a lead-screw arrangement to set the stiffness range, and a base motor that is coupled to VSM, as shown in Fig. 1. The VSM consists of two cam followers, a cam that contains a pair of cam slots placed antisymmetric to each other, and antagonistically placed nonlinear compression springs (s_1 and s_2), as highlighted in Fig. 1. One end of s_1 and s_2 is attached

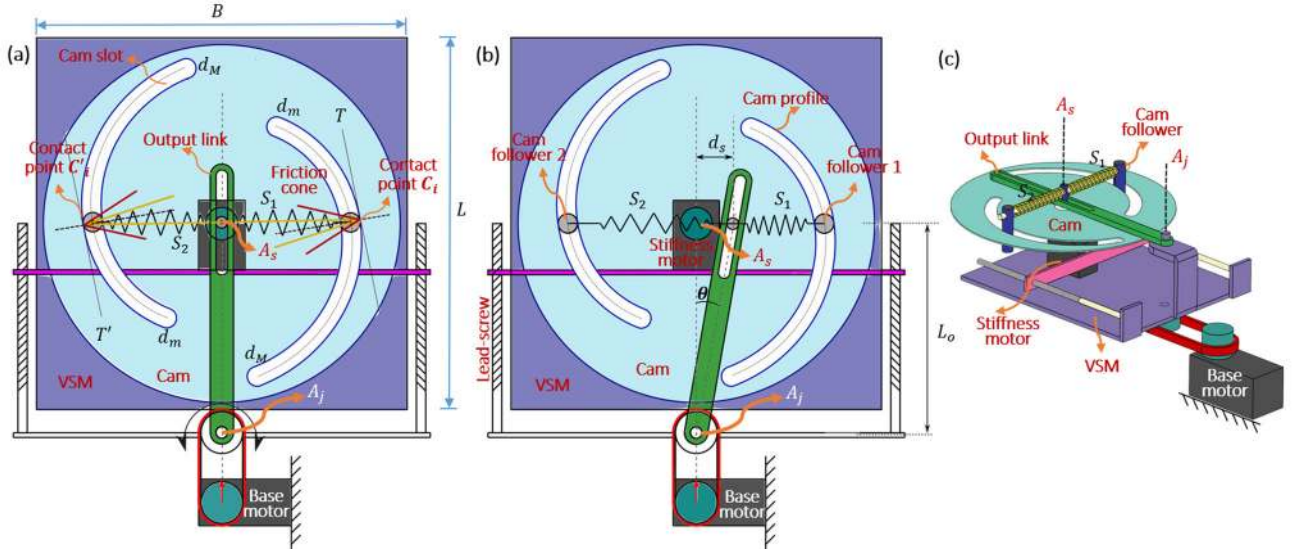

FIGURE 1. The conceptual model of the proposed VSJM: (a) output link is at the equilibrium position, (b) output link is deflected from the equilibrium position, and (c) simplified 3D model.

with the cam follower 1 and 2, respectively, and the other ends are coupled with the slotted output link. Each of the followers is constrained to move only along the horizontal direction and is configured to slide in the corresponding cam slot. A motor is attached directly to the cam for changing the joint stiffness within the set range, and we call it the stiffness motor. By actuating the base motor, the VSM box is actuated as a whole and hence changes the equilibrium position of the output link. By actuating the stiffness motor, the deflection of the nonlinear springs is controlled; hence, change in stiffness is accomplished. In Fig. 1a, C and C' denote the contact points between the cam follower and the cam slot. The friction cones at the contacts C and C' are utilized to counteract the moment about the cam center due to vertical offset between C and C' when the output link is in the equilibrium position, as illustrated in Fig. 1a.

According to Nguyen's criterion [39], if there exists a line that connects the two contact points and if that line is an interior of the friction cone, then the system of forces are balanced [40]. In the proposed design, the cam profile is synthesized based on this criterion to meet the static equilibrium condition at the contacts without powering the stiffness motor (this would be discussed in detail in Sec. III). When the output link is displaced from the equilibrium position, as depicted in Fig. 1b, the springs are deflected, and a restoring moment is generated. The change in stiffness range is achieved by manually varying the offset L_o between the axis that passes through the stiffness motor A_s and joint axis A_j, with the help of the lead screw arrangement. Reducing the offset L_o makes the joint more complaint and increases the range of the angular displacement of the output link. On the other hand, increasing the offset results in a stiffer joint and reduces the range of the output link angular displacement without changing or replacing any of the components. Further, within the manually set range, the stiffness can be adjusted electronically by rotating the cam without disturbing the equilibrium position of the output link. It enables the system to be more compact. The nonlinear relationship between the force and deflection of the springs could be achieved by various means, like variable pitch springs, stacking multiple linear springs with different stiffnesses, and so on. For simplicity, we have used two different springs with different stiffnesses that are connected in series as a single spring element. Also, the magnitude of force/torque at the joints can be sensed from the deflection of the passive element without using any force/torque sensor. This enables the system to be more affordable, especially in applications like rehabilitation robotics.

III. WORKING PRINCIPLE AND MATHEMATICAL MODEL

A. WORKING PRINCIPLE

The proposed VSJM has a base motor for changing the equilibrium position of the output link, and a stiffness motor that is encapsulated within the VSM to change the joint stiffness. When the cam is rotated in Clockwise (CW)/ Counterclockwise (CCW) direction, the nonlinear springs are compressed/relaxed, which exert forces F_{s1} and F_{s2} at the corresponding contact points C and C', respectively. When the output link is at equilibrium, and if the cam profile is noncircular, the line connecting both contact points would not be coincident with the forces F_s exerted due to the deflection of springs. As a result, the force F_s acting horizontally at the contact would have the components along tangent and normal direction at C and C'. The offset between the two contact points along the vertical direction generates a moment about the cam center. As a consequence, if no external force exists, the cam rotates CCW until the cam followers reach the extreme cam position d_M. One way of counteracting this moment is by applying the torque using the stiffness motor

which is directly coupled with the cam. But this requires the motor to be powered even when the output link is stationary. The second way of achieving the torque equilibrium is by making the forces due to springs coincide with the contact normal forces at the contacts. In this case, the trivial solution for the cam profile is a circle, where the force/torque equilibrium can be maintained. But, in this case, change in stiffness would not be possible, as the springs would not deflect. Therefore, a noncircular cam profile has to be found to change the stiffness as the cam moves, and, at the same time, retain the cam position from the unbalanced forces at the contacts.

In this paper, we have proposed the design of the VSJM to counteract the unbalanced forces at the contacts if the cam profile is noncircular. Thus, the continuous actuation of the stiffness motor could be avoided. The cam profile has been designed to maximize the change in stiffness as the cam rotates and to maintain static equilibrium. This ensures that no external work needs to be done to resist the moment generated due to offset in antagonistic contact forces under no-load conditions. The details of the static equilibrium and synthesizing of the cam profile will be discussed in the following sections.

B. CAM PROFILE SYNTHESIS

When the output link of the VSJM is not displaced from its equilibrium position, the cam and the cam follower need to be in static equilibrium. The cam profile is synthesized based on this criterion. How to achieve the static equilibrium and how to synthesize the cam profile to maximize the change in the stiffness of the springs during the movement of the cam follower are presented here.

The free-body diagram of the cam follower in contact with the cam profile is shown in Fig. 2. Let O_1 and O_2 be the cam center and center of the follower, respectively. The point of contact between the follower and the cam profile is shown as C. The line AC, normal to the tangent T at C, intersects at A with $O_1A||T$, and forms a right-angled triangle ΔO_1AC. Let λ be the interior angle, r_1 and r_2 be the length of the sides of ΔO_1AC, and φ be the cam angle measured from the x-axis, as shown in Fig. 2. The components of nonlinear spring force F_s at the contact, C, are the normal force F_N and tangential force F_T. Frictional force F_f is acting along T in the direction opposite to F_T. For the cam to be in static equilibrium, the moment generated due to the normal contact force should be balanced by the moment due to the frictional force, as shown in (1).

$$F_f r_1 = F_N r_2 \tag{1}$$

From Fig. 2, r_1 and r_2 are trigonometrically related to λ and Equation (1) can be rewritten as

$$\frac{F_f}{F_N} = \frac{r_2}{r_1} = \text{Tan}\,(\lambda) \tag{2}$$

Assuming the relationship between the spring stiffness K_s and the spring deflection d_s is monotonic, the change in spring deflection with respect to cam rotation should be maximized

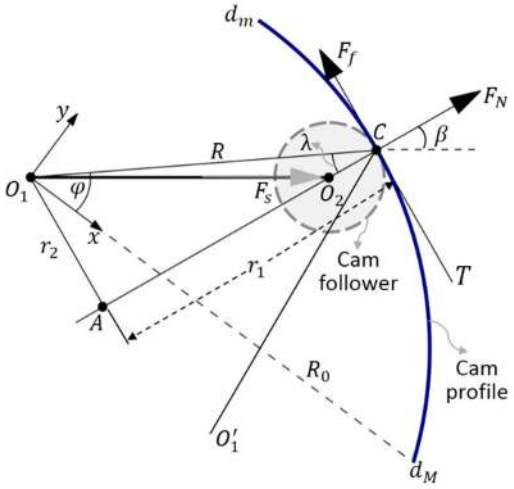

FIGURE 2. Free body Diagram showing the contact point and the contact forces between the cam follower and cam profile.

to maximize the change in joint stiffness. This implies that for any given cam angle φ, a cam profile that has maximum β is desired, where β is the angle between the contact normal and the horizontal axis. From Fig. 2, one can observe that an increase in $\beta \in [0, \pi/2)$ results in an increase in λ. From (2), λ turns out to be the friction angle, hence, there exists a maximum, λ^*, for λ that depends on the type of materials in contact. The desired cam profile is obtained when $\lambda = \lambda^*$ for every contact point. Hence, if μ is the static friction coefficient,

$$\text{Tan}\,(\lambda^*) = \frac{F_{fmax}}{F_N} = \mu \tag{3}$$

To attain Nguyen's criterion [39], we have imposed that one of the edges of friction cone, i.e., CO_1 has to pass through the cam center so that the moment would be compensated by the opposite contact. In other words, the edge CO_1 of the friction cone at C should coincide with the edge $C'O_1$ of friction cone at the contact C' between cam follower2 and cam profile, as illustrated in Fig. 1. With this, static equilibrium is achieved by constraining the motion of cam through a set of contact points with friction. Assume that there are no external forces applied to the output link, then the contact forces at every point contact pairs in the cam profile have to balance each other so that the cam remains in the static equilibrium condition.

Since the cam consists of two cam slot profiles with a finite length, each profile has two extreme positions, that are, d_m and d_M, where the length of the spring is minimum and maximum, respectively. The cam follower remains in this extreme position when the springs are either in a fully compressed or expanded state. When the cam follower is at one of the extremities of the cam angle, say at d_M, then contact normal force (F_N) would be minimal because of less deflection of the spring. Otherwise, F_N would be maximum if the spring is fully compressed. The minimal normal force

constitutes less tangential force; therefore, a less frictional force is sufficient to counteract.

To find the appropriate cam profile to meet the design requirements, consider an imaginary profile which is highlighted in blue color, as shown in Fig. 3. A coordinate frame, O_1, is attached to the center of the cam, whose x-axis passes through the initial point of the cam profile, d_M, as shown in Fig. 3. The cam angle φ is measured from x -axis to the line joining O_1 and the contact point C_i. Assume that the contact point has shifted from C_i to C_k when the cam is rotated in a CW direction, with an infinitesimal angular displacement $d\varphi$, as illustrated in Fig. 3. The distance from the contact point C_i to the cam center is denoted by R. In order to determine the relationship between friction angle and cam profile, a right-angled triangle can be formed where the vertex C_k is at $(R - dR)$ from O_1 and follows the below trigonometric relation.

$$Cot\,(\gamma) = -\frac{1}{R}\frac{dR}{d\varphi} \tag{4}$$

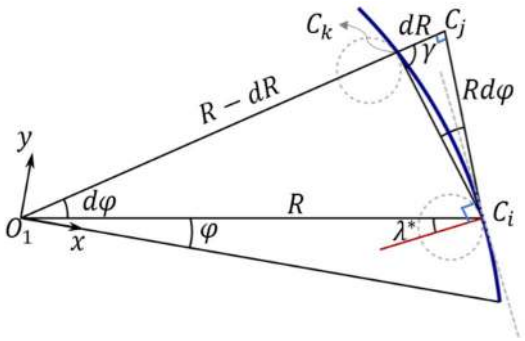

FIGURE 3. Small-angle approximation for synthesizing the cam profile.

The negative sign is because the length variable R decreases with an increase in cam angle φ, as compression springs are used. From Fig. 3, the friction cone angle λ^*, and γ can be related by

$$\gamma = \pi/2 - \lambda^* \tag{5}$$

Substituting (5) in (4), we get

$$Cot\left(\pi/2 - \lambda^*\right) = \mathrm{Tan}\left(\lambda^*\right) = -\frac{1}{R}\frac{dR}{d\varphi} \tag{6}$$

Using (3), the above equation can be rewritten as

$$\frac{dR}{d\varphi} = -R\mu \tag{7}$$

Solving the above differential equation, we obtain the length between the cam center and contact point, R as

$$R = R_0 e^{-\mu\varphi} \tag{8}$$

From the expression, R is exponentially related to the coefficient of friction and cam angle. When $\varphi = 0$, then $R = R_0$, which is the initial distance between O_1 and d_M. Using (8), we have found the cam profile for different μ values. Also, the same has been illustrated using a polar plot where the concentric circles and the radial lines represent the length R and cam angles, respectively, as given in Fig. 4 (this has been plotted for a fixed value of $R_0 = 35$mm). As pointed out earlier, the relation between the cam profile and the coefficient of friction is established, now we proceed to explain the design procedure as follows.

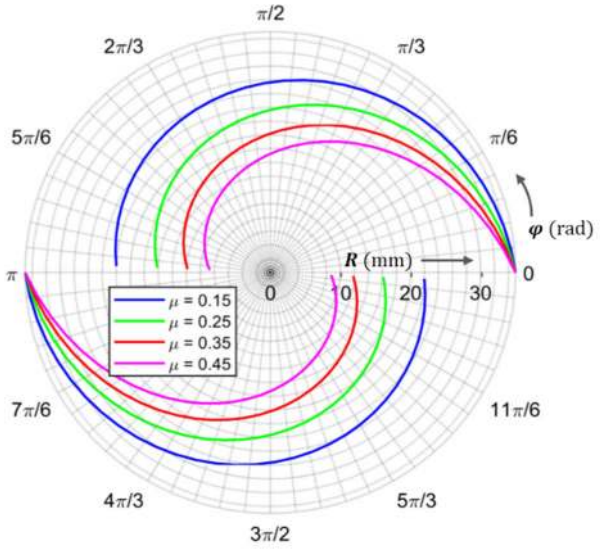

FIGURE 4. Cam profile for various friction coefficients and fixed $R_0 = 35mm$.

C. DESIGN PRINCIPLE

The following are the design principle for the proposed VSJM:

Design Objective:

(a) The module has to be made compact for practical implementation in robotic joints.

(b) The cam should remain in statically stable condition when the output link is in equilibrium condition.

(c) Power consumption should be less than the conventional variable stiffness mechanisms.

Design Specifications:

(a) To ensure the first design objective, the length (L) and breadth (B) of VSM were chosen to be 120 *mm* and 140 *mm*.

(b) The mechanical stiffness K_M should vary as a function of the cam angle φ (assuming that output link is in equilibrium). For simplicity, the mechanical stiffness K_M is assumed to be K_{M1} for the cam angle range $\varphi \in [0, \varphi^1)$ and K_{M2} for the next cam angle range $\varphi \in [\varphi^1, \varphi^2]$, where φ^1 is the intermediate cam angle and φ^2 is the maximum cam angle, i.e.,

$$K_M = \begin{cases} K_{M1} = 3Nm/rad, & \text{For } \varphi \in [0, \pi/2) \\ K_{M2} = 20Nm/rad, & \text{For } \varphi \in [\pi/2, 5\pi/6] \end{cases}$$

(c) The maximum output link angular displacement for a minimum stiffness of VSJM (K_{M1}) is chosen to be $\theta_{max} = 25°$.

Design Methodology:

To attain the above requirements, the methodology we followed for designing the proposed VSJM is described below.

1. Based on the length and width, the parameter L_o is decided not to exceed half the length of the VSM box, i.e., $L_o < L/2$.

2. Based on the width, B, of the VSM, the length of the spring at minimum stiffness K_M, can be found. This will be equal to R_0.

3. Using (8), for the given friction coefficient μ, the equation for the cam profile $R(\mu, \varphi, R_0)$ has been found.

4. For each section of cam angle φ^i, the stiffness of the spring section (K_s^i) has been found from the mechanical stiffness (K_M), and the relationship is described in Sec. IV.

5. The maximum deflection of the spring (d_s) is found from the maximum output link angle at K_{M1} (when cam angle $\varphi = 0$).

6. The nonlinear spring deflection d_s versus spring stiffness K_s has been found using the cam profile equation (8).

7. From step 6, the spring sections are designed [41]. Further details on spring design is discussed in Section V.

To minimize the potential energy associated with the springs, the cam follower would slide along the cam profile. By maintaining the equilibrium at the edges of the cone, even a small disturbance at the contact would lead to breaking the static equilibrium. To circumvent this issue in the prototype, the cam profile has been found for the lesser friction coefficient than the actual one.

IV. STATIC ANALYSIS

One of the main contributions of this work is to find the cam profile to maintain static equilibrium, as discussed in the previous sections. Utilizing this cam profile, two VSJM designs are presented, which are designated as Design1 and Design2. Design1 is equipped with two springs, a lead-screw arrangement to set the stiffness range manually, and a cam mechanism. Design2 is a simplified version of Design1 and is equipped with four springs (to increase the overall mechanical stiffness) and a cam mechanism. The lead-screw mechanism is not included in Design2 to simplify the fabrication process. In this section, the relationship between the joint torque and stiffness has been established for both of the designs, as described below.

A. STATIC ANALYSIS: DESIGN1

The free body diagram in Fig. 5a shows the angular displacement of the output link and the corresponding restoring forces generated by the two springs. The L_o parameter that can be varied through a lead-screw arrangement, and the displacement of the output link angle, measured from the equilibrium position d_l, are shown in Fig. 5a. Under the static equilibrium condition, the torque experienced about the joint axis A_j can be calculated with the help of Fig. 5a, as given below.

$$\tau = (F_{s2} - F_{s1})L_o \tag{9}$$

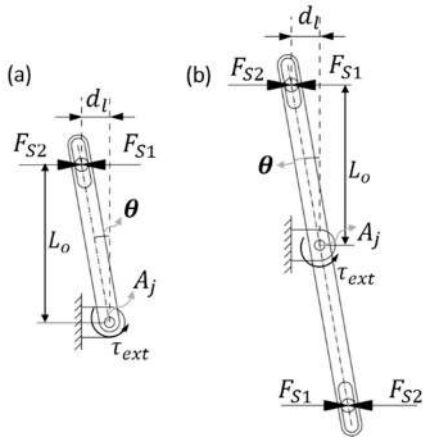

FIGURE 5. Shows the free body diagram of output link and the associated spring forces for: (a) Design1 and (b) Design2.

Let d_c and d_l be the deformation of the spring due to the displacement of the cam and output link, respectively, then

$$\tau = (K_s\,(d_c + d_l) - K_s\,(d_c - d_l))\,L_o \tag{10}$$

After simplification,

$$\tau = 2K_s d_l L_o \tag{11}$$

From Fig. 5a, we obtained the trigonometric relation $d_l = L_o Tan(\theta)$, and substituted in (11) as

$$\tau = 2K_s L_o^2 Tan(\theta) \tag{12}$$

The instantaneous stiffness of the overall mechanism K_M is

$$K_M = \frac{\partial \tau}{\partial \theta} = 2K_s L_o^2 Sec^2(\theta) \tag{13}$$

From (13), one can observe that the mechanical stiffness K_M is a function of output link displacement θ, spring stiffness K_s, and offset L_o. The relation between K_M, L_o and φ is shown in Fig. 6, where L_o is varied from 40 to 60 mm. For the plot shown in Fig. 6, the spring stiffness is assumed to be linearly related to spring deflection, i.e., a quadratic relationship between spring force and deflection.

For a smaller angle displacement of the output link, the mechanical stiffness becomes,

$$K_M \approx 2K_s L_o^2 \tag{14}$$

B. STATIC ANALYSIS: DESIGN2

The torque experienced about the joint axis A_j for the Design2 is calculated, similar to Design1. In this design, there are four springs, and the offset L_o is fixed, as shown in Fig. 5b. Using Fig. 5b, the torque experienced is calculated, as

$$\tau = 2(F_{s2} - F_{s1})L_o \tag{15}$$

The instantaneous stiffness of the overall mechanism K_M is

$$K_M = \frac{\partial \tau}{\partial \theta} = 4K_s L_o^2 Sec^2(\theta) \tag{16}$$

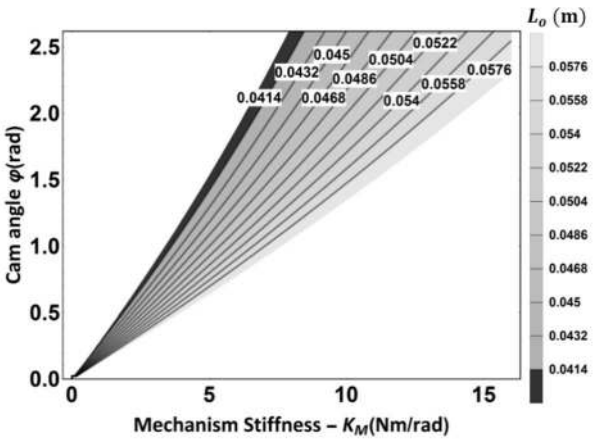

FIGURE 6. Shows the relation between the mechanical stiffness, cam angle, and the variable offset L_o for the Design1.

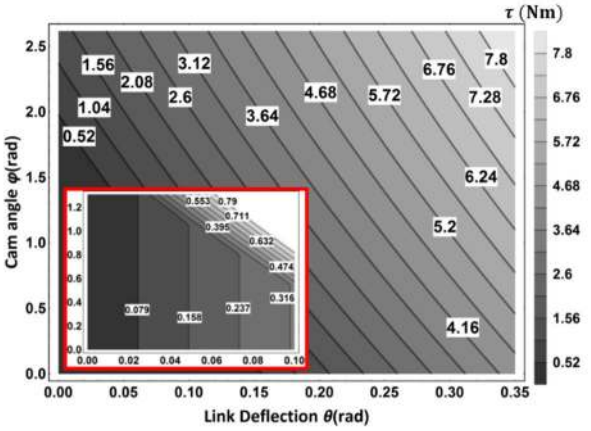

FIGURE 7. Shows the relation between the torque, cam angle, and link angle θ (offset L_o is fixed) for the Design2. The zoomed view shows the change of torque even for a small output link deflection.

From (16), it can be seen that the mechanical stiffness of Design2 is increased by a factor of 2 for the same L_o. Since L_o is fixed in this case, K_M is the function of θ and K_s. The relationship between φ, θ, and τ is shown in Fig. 7. Here, it is assumed that, $K_s = k_1$ for spring deflection $d_s \leq d_1$ and $K_s = k_2$ for $d_1 < d_s \leq d_2$, where $d_1 = 10$ mm and $d_2 = 22$ mm.

V. MECHANICAL DESIGN AND PROTOTYPE

In this section, we present the detailed design, and CAD modeling of the VSJM prototypes Design1 and Design2, as follows.

A. DESIGN1

In this design, two ways of changing the stiffness have been proposed to obtain a higher stiffness range, keeping the mechanism as compact as possible. The design consists of an electronically powered cam mechanism to actively change or control the joint stiffness and a lead-screw arrangement to adjust the stiffness range manually. The detailed CAD assembly is shown in Fig. 8a. The input link ① and output link ② are pivoted at A_j, which is coincident with the base motor ③ axis. A position-controlled Dynamixel^{TM} motor ④ is directly coupled with the cam ⑤. The cam-followers ⑥a and ⑥b are rigidly attached with the first ⑦ and third ⑧ sliding blocks, which are engaging in the antagonistic

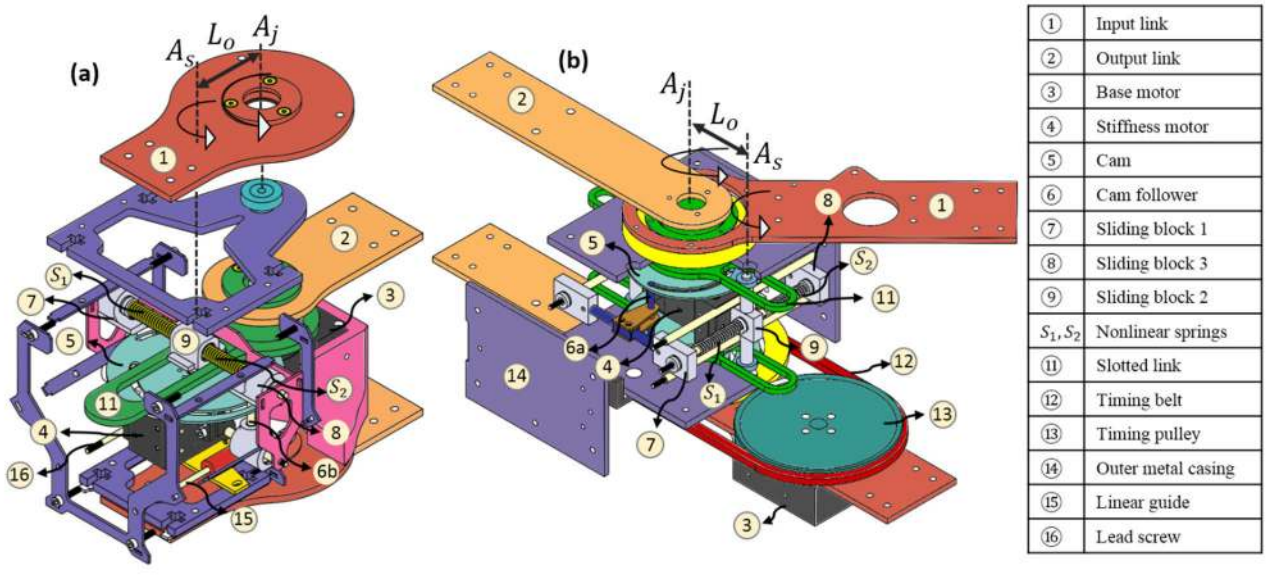

①	Input link
②	Output link
③	Base motor
④	Stiffness motor
⑤	Cam
⑥	Cam follower
⑦	Sliding block 1
⑧	Sliding block 3
⑨	Sliding block 2
S_1, S_2	Nonlinear springs
⑪	Slotted link
⑫	Timing belt
⑬	Timing pulley
⑭	Outer metal casing
⑮	Linear guide
⑯	Lead screw

FIGURE 8. The CAD model of the proposed VSJM: (a) Design1 – with two springs, a cam mechanism, and a lead-screw arrangement, (b) Design2 – with four springs, cam mechanism, and without the lead-screw arrangement.

arrangement with one end of the springs ⑩a and ⑩b. The other end of the springs ⑩a and ⑩b are mechanically linked to a second sliding block ⑨. The sliding blocks ⑦ and ⑧ are configured to compress the springs to vary the stiffness by actively rotating the cam ⑤ using the stiffness motor ④. The second sliding block ⑨ is constrained by a linear slot provided in the output link ② and is allowed to move only along the axis of the springs. The lateral motion of the second block ⑨ takes place when the output link is displaced (d_s) from the equilibrium position. The metal enclosure ⑭ is used to assemble the base motor, lead screw ⑯, and linear guide ⑮. By manually rotating the lead screw, the variable stiffness mechanism subassembly is moved by a distance L_o that is measured between A_j and A_s. The entire cam mechanism is placed on the lead-screw, which is configured to vary the offset L_o between the axis of the joint actuator and the second block ⑨, to modify the range of stiffness and is termed as a first stiffness range.

B. DESIGN2

This design excludes the lead-screw arrangement; thus, the change in stiffness is solely due to the cam mechanism. In this, the axis of the joint actuator and the axis of stiffness actuator are made coincident, as shown in Fig. 8b. To make the device compact and to increase force and stiffness range, a total of four nonlinear springs are used. An antagonistic spring pair (S_1,S_2) is placed at either side of the stiffness motor. Apart from that, two cams and two double-slotted links (kept parallel) are used, one on top and other on the bottom of the stiffness motor. This is to nullify the moments of sliding block ⑨ and cam follower about the pivoted point. The output link is rigidly attached to the slotted links, and an encoder (Broadcom®, AEAT-601B-F06) is attached to the output link whose axis is coincident with A_j. The simplified schematic of the design is shown in Fig. 9 for the different angular displacements of the output link. The nonlinear characteristics of springs are obtained by serially connecting two springs of different stiffness values. All four springs have the same force-deflection characteristics. The deflection of the spring pairs (S_1, S_2) could be observed in Fig. 9. The design details of the springs have been discussed in the next subsection.

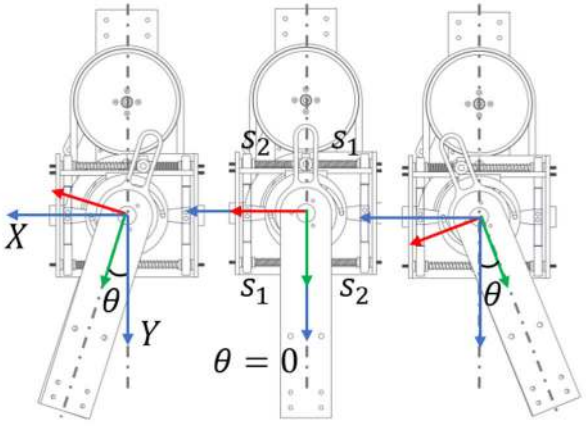

FIGURE 9. Shows the different configurations of output link for Design2 and corresponding spring deflections.

C. SPRING DESIGN

The nonlinear characteristic of a spring can be achieved in different ways. One of the methods is to use multiple linear springs with different stiffnesses that are connected in series. The pictorial representation of the two linear compression springs with different stiffnesses connected serially, which act as a spring element S_1 and S_2, is shown in Fig. 10a. The one with the relatively lesser stiffness is called soft spring, and the other with the higher stiffness is called hard spring. The specifications of the hard and soft springs are given in Table 1. In order to avoid buckling while displacing one end of the spring, the springs are inserted onto a cylindrical rod. The effective stiffness of the serially connected springs is the net stiffness considering both the hard and soft springs until the soft spring completely shuts. After the soft spring completely shuts, the effective stiffness of the serially connected springs is the stiffness of the hard spring itself. Let K_{hs} be the hard spring stiffness, K_{ss} be the soft spring stiffness, s is the displacement of the spring, s_1 is the maximum displacement at which the stiffness changes from K_e to K_{hs}, and s_2 is the maximum displacement of the serially connected springs (both soft spring and hard spring). The effective spring stiffness K_S can be found by

$$K_s = \begin{cases} K_e & s \in [0, s_1] \\ K_{hs} & s \in [s_1, s_2] \end{cases} \tag{17}$$

where, $K_e = \frac{K_{ss}K_{hs}}{K_{ss}+K_{hs}}$.

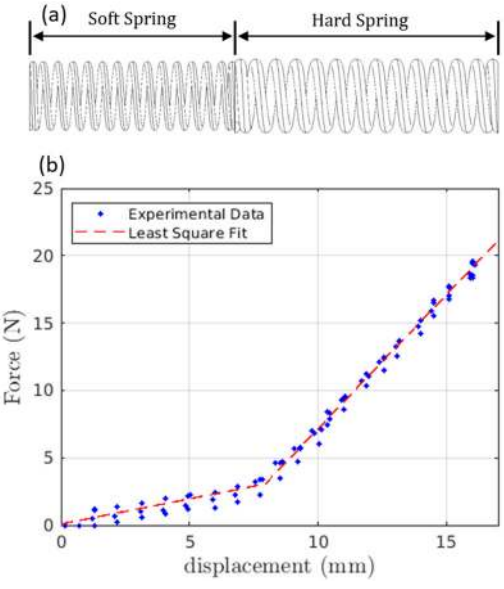

FIGURE 10. (a) Shows two serially connected springs named hard and soft springs, (b) shows the force-displacement characteristic of the serially connected springs.

TABLE 1. Spring specifications.

Parameters	Soft spring	Hard spring
Inner diameter (mm)	5.9	5.9
Wire diameter (mm)	0.6	1.1
Number of Active Turns	13	12
Free Length (mm)	20	25
Material	SAE 1070-1090	SAE 1070-1090
Stiffness (N/m)	459	1994

The resultant force-displacement characteristics of the serially connected springs are shown in Fig. 10b. It can be seen that effective spring stiffness changes from K_e to K_{hs}, as given in (17).

VI. EXPERIMENTAL RESULTS AND DISCUSSION

The fabricated prototype of VSJM (Design2) is shown in Fig. 11. The encapsulated VSM module, input and output links, and the controller elements are shown in Fig. 11a. The overall dimensions of the VSM are shown in Fig. 11b. The total power consumption of the system depends on the number of electrically powered components. In general, the two motors that are used to change the stiffness and joint angle are the major power-consuming elements in the system. The introduction of additional electromechanical components like brake or clutch would increase the stiffness range. However, this leads to an increase in power consumption, introduces propagation delay, and directly affects the compactness. In the proposed design, it is noteworthy to mention that, due to the optimized cam profile, the stiffness motor need not be powered as long as the output link is in the equilibrium position. Hence, the continuous need for powering the stiffness motor is avoided, which results in reduced power consumption. Besides, due to the cam mechanism, changing the stiffness is quick compared to the lead-screw arrangement. Experiments were performed on the prototype fabricated based on the Design2 to show the effectiveness of the proposed design. The results are valid for Design1 also and could be extended for further analysis. As a first step, we present the comparison and validation of the theoretical and experimental data. Then, we present the results obtained from the task of a hammering application and discuss the associated algorithm used.

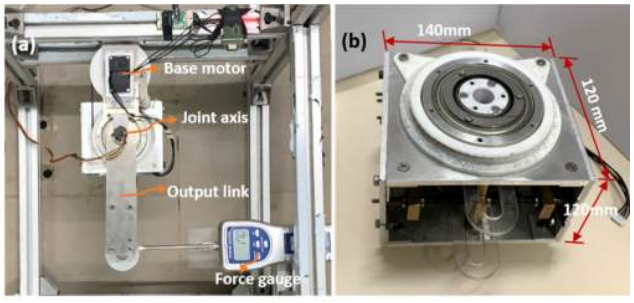

FIGURE 11. Shows the fabricated prototype of VSJM (a) encapsulated with VSM and (b) VSM with the major dimensions.

To validate the model of variable stiffness mechanism, the theoretical value of the mechanical stiffness K_M computed from (16) is compared with the experimental data. To conduct this experiment, a force gauge (Lutron®FG-5020) is coupled to the output link at the distance of l ($l = 0.31m$) from the joint axis, as can be seen in Fig. 11. The variable stiffness characteristic of each nonlinear spring element is realized by serially connecting two springs with different stiffness values, named soft and hard spring, with low and high spring stiffness, respectively. Initially, the output link axis, which is in the equilibrium position, has been aligned perpendicular to the axis of the force gauge, as shown in Fig. 11a. The stiffness motor and base motor used in the VSJM are Dynamixel®XH430-W350-R and XM540-W270-R, respectively. The cam angle φ is kept constant at 0°,36°,72°,108°, and 144°, and for each of these cam angles, the base motor is commanded to rotate in incremental steps against the force gauge, and then released. Since the output link motion is physically constrained by the force gauge as the base motor rotates, the output link deflects from the equilibrium position by θ. The corresponding θ is measured using the encoder, and the respective force is measured, as shown in the test setup in Fig. 11. The measured force is converted into torque which is denoted as τ_{ext}. A series of five experiments were conducted for each φ, and the results are reported in Fig. 12. The mean and variance of τ_{ext} is shown in solid line and shaded area, respectively, and the dotted line represents the theoretical value of τ_{ext} computed using K_M from (16) and constant distance l. As the output link displaces from its initial position, the soft spring reaches its deflection limit, followed by the hard spring. This is apparent in Fig. 12, as two different slopes, can be observed for each cam angle. When $\varphi = 0°$, both hard and soft springs contribute to the overall stiffness of the mechanism, and when the cam angle reaches $\varphi = 144°$, soft springs are completely shut, and the major contribution is due to hard springs. The occurrence of hysteresis is visible in Fig. 12 and is mainly due to the indirect belt drive actuation of the base motor and its associated compliance, as well as the friction between the mechanical components. As a result, the torque is different for upstream and downstream. The mean and variance of the mechanical stiffness (first slope and second slope as can be seen in Fig. 12), for the fixed cam angle, is reported in the top and bottom subplot of Fig. 13.

The stiffness of the VSJM can now be set using Fig. 13. The cam angle φ is found for a desired joint stiffness using the plot in Fig. 13. This cam angle is then commanded to the stiffness motor, which is a position-controlled servo motor. Thus, the stiffness control of the proposed VSJM is trivial as it just requires the position to be commanded, and the stiffness will be maintained at the commanded level by the cam itself due to its design, as explained in the previous sections.

Table 2 compares the specifications of the proposed VSJM with other existing actuators. It would not be easy to draw

TABLE 2. Comparison of variable stiffness actuators.

Specifications	Proposed VSM	BpVSJ [23]	MACCEPPA [26]	SVSA [20]	AwAS [16]
Range of motion (Deg)	$\pm 150^o$	#	$\pm 150^o$	$\pm 180^o$	$\pm 120^o$
Angular deflection (Deg)	$\pm 24.5^o$	Less than 10^o*	$0 - 60^o$	$\pm 45^o$	$\pm 14^o$
Stiffness range (Nm/rad)	2.7 – 19.2	28.648, 57.29, and 114.59	5 – 110	1.72 – 150.56	30 – 1500
Dimensions (mm)	140 x 120 x120	230 (Diameter)	#	300 (Diameter)	270 x 130
Weight (kg)	1.9 (including the weight of stiffness motor)	17.9 (gross weight)	2.4	0.9	1.8
Stiffness motor power consumption (W)	0 – 1.8	15 – 45	#	#	~ 0 – 14*
Maximum elastic energy (J)	1.26	~0.706*	27.9	3.7	3.2

* Inferred from the plot in the paper # could not be found or reported in the paper

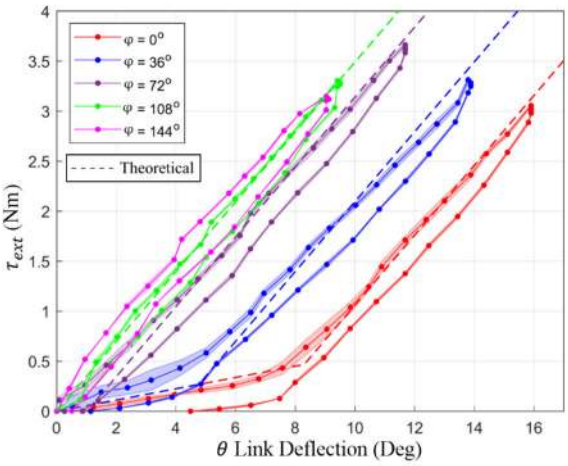

FIGURE 12. Shows the comparison between the experimental data and theoretical values, i.e., the relationship between output link angle deflection and external torque for the fixed cam angles. The solid line and shaded area represent the mean and variance of the experimental data, and the dotted line represents the theoretical value.

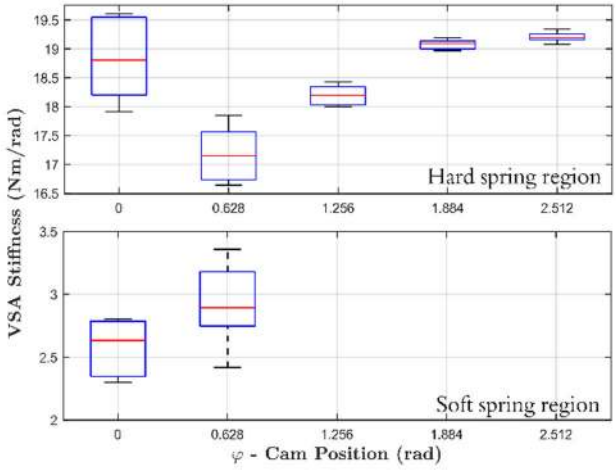

FIGURE 13. Shows the mechanical stiffness for different cam angles.

the best configuration out of many designs available in the prior art. However, to justify the specifications of the proposed design, Table 2 could be regarded as a quantitative assessment. Comparing the dimensions of the proposed actuator with the existing VSAs (comparison is based on the cross-sectional area), it is quite evident that the VSJM is more compact. The compactness is attributed to the symmetric design of the VSM, where the four springs, two on either side of the stiffness motor, are so arranged to increase the joint stiffness as well as to reduce the space occupied by them. The stiffness motor consumes power only for changing the stiffness. At a fixed stiffness of the joint, the stiffness motor does not consume any power because of the cam profile design. The stiffness motor is observed to consume a peak current of 150mA (which gives peak power of 1.8W for 12V power supply) when it is commanded to change the stiffness from the minimum to maximum value. This power consumption is significantly less when compared to the existing actuators. The time taken for changing the stiffness from minimum to maximum was computed based on the measured speed of rotation of the stiffness motor (28 rpm) and was found to be ~90ms.

The stiffness range of the VSJM is scalable, yet, in a practical situation, the stiffness range is limited by the motor characteristics like peak torque (3.4Nm in our case) and peak excitation frequency. In this prototype, the stiffness is chosen to be less compared to other existing designs to suit the hammering application. By reducing the stiffness, the excitation frequency has been reduced. Hence the stiffness is chosen such that the actuator excitation frequency lies well within the bandwidth of the base motor.

A. HAMMERING TASK

To demonstrate the capability of the proposed design, we have considered the hammering-a-nail task where the VSJM is expected to produce an explosive movement while hammering the nail into the wooden block. For this experiment, the mechanical energy stored by the passive spring elements is utilized to generate the impulse at the time of hitting the nail. The experimental setup for the same is shown in Fig. 14. The VSA has been mounted on the fixture and is operated in the horizontal plane. A metallic hammer is attached to the output link to hit the nail head. A wooden block is placed in the vertical plane and is rigidly fixed with the fixture. A nail

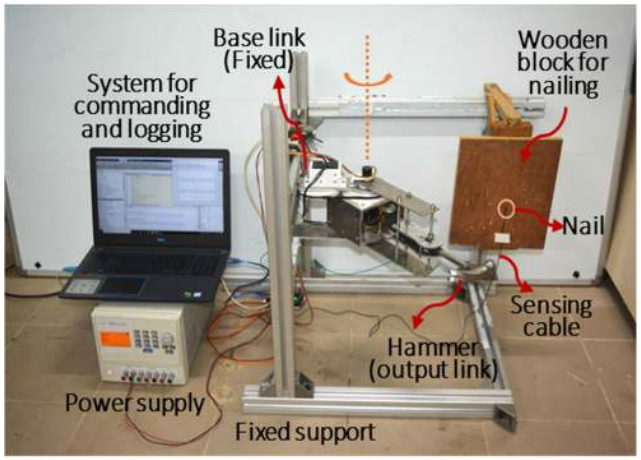

FIGURE 14. Shows the experimental setup for hammering task.

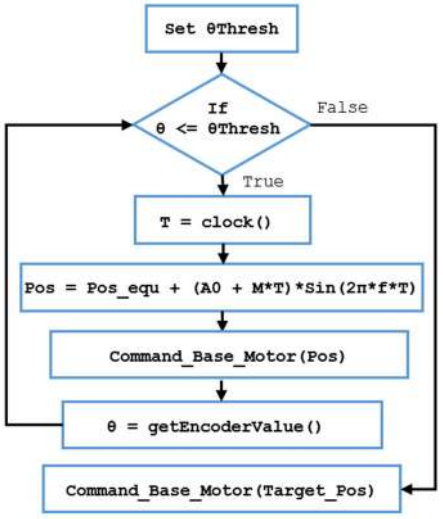

FIGURE 15. Shows the flow chart describing the hammering task.

is positioned at the wooden block with a minimal penetration and is ensured that its axis would be intersecting with the hammerhead plane during the time of impact. By doing so, the maximum force would be imparted, and the undesired displacement of the nail would be avoided. A sensing probe is connected with the nail to find the time of impact t_{im}. The time of impact is calculated from the instant when the command signal is given to the base motor until the time instant the impact happens. The impact is sensed by monitoring the state of the continuity probe, which triggers an interrupt signal to the controller, to find t_{im}. The output link is equipped with an appropriate quadrature encoder, and the microcontroller reads the signal. The controller transmits the encoder value and the sensing probe state to the system through serial communication.

The algorithm followed to achieve the maximum velocity of the hammer at the final position θ_f, i.e., just before hitting the nail or the point of impact, is illustrated in the flow chart shown in Fig. 15. The hammer connected with the output link

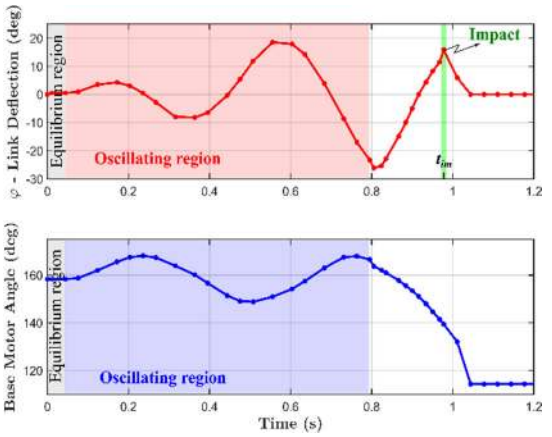

FIGURE 16. The red and blue regions represent the oscillation of output link about the equilibrium position and base motor about the initial position, respectively. The time of impact is indicated in green color.

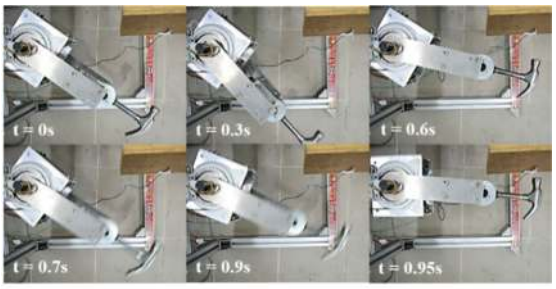

FIGURE 17. Shows the image sequence of the hammering task at different time instants starting from the equilibrium position till the final impact.

is excited by oscillating the base motor about an equilibrium position (indicated as a gray region in Fig. 16) to energize the elastic elements. A sinusoidal waveform with a linearly increasing amplitude (Pos, as given in Fig. 15) is given as the input command to the position-controlled base motor, as indicated in the blue region, in Fig. 16. The values of the parameters used for the experiment that define the sine wave are $f = 1.7$Hz, M $= 35.160°$ and A0 $= 13.2°$. The equilibrium position (Pos_equ $=160°$ CCW from the negative Y-axis in Fig. 9) of the VSJM has been carefully chosen to be away from the position of the nail, i.e., point of impact so that the maximum deflection of the output link during excitation would not be affected while energizing the mechanism. The system will be in the oscillating phase until the output link angle is more than the threshold angle (θThresh $= 23°$). The oscillation of the output link with respect to the base motor oscillating trajectory is shown in red color at the top of Fig. 16. The image sequence in Fig. 17 illustrates the configuration of VSJM at different time instances. As the output link reaches the maximum angle, which is monitored by the encoder, all the gained kinetic energy is converted into potential energy with respect to the output link equilibrium position. At the same instant of time, at $t \approx 0.8s$, a goal state (Target_Pos $= 114°$) is commanded to the position-controlled base motor, to move towards the nail head.

When the hammerhead hits the nail, the corresponding impact time (t_{im}) is recorded using the sensing probe and is highlighted in Fig. 16. The length of penetration of the nail into the wooden block is measured manually, and a penetration of 2 mm is observed for each hit. From this, we have experimentally shown how the variable stiffness joint module could be utilized to perform explosive movements. For this particular experiment, the cam angle has not been modulated. The idea of finding the optimal stiffness profile to maximize the impulsive forces by changing the cam angle would be addressed in future work.

VII. CONCLUSION

Although many VSA designs exist in the literature, only a few of them have considered the reduction of power consumption as a design requirement. Of them, the majority of the designs use lead screw arrangement for changing the stiffness. Therefore, powering the stiffness motor continuously is not required, and thus consumes lesser power when compared to other designs. However, the change in stiffness would not be quick due to the lead screw arrangement. In order to tackle these issues, a new design of a variable stiffness joint module has been presented. In this, the cam has been designed to maintain its position without powering the stiffness motor when the output link is in the equilibrium position. The cam profile has been synthesized considering the friction cones at the contacts between the cam and cam follower to achieve a static equilibrium condition. Therefore, the moment due to normal contact forces is balanced by the moment due to friction at the contacts. Hence, an external torque (i.e., powering the stiffness motor) is not required to retain the cam position since the forces at the contact points are statically stable. This has resulted in the stiffness motor having zero power consumption to maintain a stiffness level and only consuming power for changing the stiffness. The usage of a cam for changing the stiffness has also resulted in the mechanism being able to change the stiffness quickly unlike other existing VSAs which use lead-screw mechanism for changing the stiffness. The VSJM takes only 90ms to change the stiffness from minimum to maximum, however, the time can be further reduced by using a higher speed motor. In addition to that, the possibility of changing the stiffness by two different settings as in Design1 makes the actuator system compact and increases the mechanical stiffness range. Though the theoretical results for both the designs are presented, experiments are conducted on the Design2 prototype. These results are applicable for Design1 as well since the design procedure behind the variable stiffness mechanism is the same for both the designs. Finally, the hammering task has been demonstrated to show the capability of VSJM to generate explosive movements, where nail penetration as high as 2mm per hit was achieved.

REFERENCES

[1] A. Bicchi and G. Tonietti, "Fast and 'soft-arm' tactics," *IEEE Robot. Autom. Mag.*, vol. 11, no. 2, pp. 22–33, Jun. 2004, doi: 10.1109/MRA.2004.1310939.

[2] G. A. Pratt and M. M. Williamson, "Series elastic actuators," in *Proc. IEEE/RSJ Int. Conf. Intell. Robots Syst.*, Aug. 1995, pp. 399–406, doi: 10.1109/IROS.1995.525827.

[3] T. Morita and S. Sugano, "Development of one-DOF robot arm equipped with mechanical impedance adjuster," in *Proc. IEEE/RSJ Int. Conf. Intell. Robots Syst.*, Aug. 1995, pp. 407–412, doi: 10.1109/IROS.1995.525828.

[4] D. Braun, M. Howard, and S. Vijayakumar, "Optimal variable stiffness control: Formulation and application to explosive movement tasks," *Auton. Robots*, vol. 33, no. 3, pp. 237–253, Oct. 2012, doi: 10.1007/s10514-012-9302-3.

[5] S. Wolf, G. Grioli, O. Eiberger, W. Friedl, M. Grebenstein, H. Hoppner, E. Burdet, D. G. Caldwell, R. Carloni, M. G. Catalano, D. Lefeber, S. Stramigioli, N. Tsagarakis, M. Van Damme, R. Van Ham, B. Vanderborght, L. C. Visser, A. Bicchi, and A. Albu-Schaffer, "Variable stiffness actuators: Review on design and components," *IEEE/ASME Trans. Mechatronics*, vol. 21, no. 5, pp. 2418–2430, Oct. 2016, doi: 10.1109/TMECH.2015.2501019.

[6] N. G. Tsagarakis, I. Sardellitti, and D. G. Caldwell, "A new variable stiffness actuator (CompAct-VSA): Design and modelling," in *Proc. IEEE/RSJ Int. Conf. Intell. Robots Syst.*, Sep. 2011, pp. 378–383, doi: 10.1109/IROS.2011.6095006.

[7] A. Jafari, N. G. Tsagarakis, and D. G. Caldwell, "A novel intrinsically energy efficient actuator with adjustable stiffness (AwAS)," *IEEE/ASME Trans. Mechatronics*, vol. 18, no. 1, pp. 355–365, Feb. 2013, doi: 10.1109/TMECH.2011.2177098.

[8] A. Jafari, N. G. Tsagarakis, I. Sardellitti, and D. G. Caldwell, "A new actuator with adjustable stiffness based on a variable ratio lever mechanism," *IEEE/ASME Trans. Mechatronics*, vol. 19, no. 1, pp. 55–63, Feb. 2014, doi: 10.1109/TMECH.2012.2218615.

[9] S. S. Groothuis, G. Rusticelli, A. Zucchelli, S. Stramigioli, and R. Carloni, "The variable stiffness actuator vsaUT-II: Mechanical design, modeling, and identification," *IEEE/ASME Trans. Mechatronics*, vol. 19, no. 2, pp. 589–597, Apr. 2014, doi: 10.1109/TMECH.2013.2251894.

[10] W. Wang, X. Fu, Y. Li, and C. Yun, "Design and implementation of a variable stiffness actuator based on flexible gear rack mechanism," *Robotica*, vol. 36, no. 3, pp. 448–462, Mar. 2018, doi: 10.1017/S0263574717000492.

[11] Z. Li, W. Chen, and S. Bai, "A novel reconfigurable revolute joint with adjustable stiffness," in *Proc. Int. Conf. Robot. Automat. (ICRA)*, May 2019, pp. 8388–8393, doi: 10.1109/ICRA.2019.8793906.

[12] G. K. Klute, J. M. Czerniecki, and B. Hannaford, "McKibben artificial muscles: Pneumatic actuators with biomechanical intelligence," in *Proc. IEEE/ASME Int. Conf. Adv. Intell. Mechatronics*, Sep. 1999, pp. 221–226, doi: 10.1109/AIM.1999.803170.

[13] D. G. Caldwell, G. A. Medrano-Cerda, and M. Goodwin, "Control of pneumatic muscle actuators," *IEEE Control Syst. Mag.*, vol. 15, no. 1, pp. 40–48, Feb. 1995, doi: 10.1109/37.341863.

[14] R. Schiavi, G. Grioli, S. Sen, and A. Bicchi, "VSA-II: A novel prototype of variable stiffness actuator for safe and performing robots interacting with humans," in *Proc. IEEE Int. Conf. Robot. Automat.*, May 2008, pp. 2171–2176, doi: 10.1109/ROBOT.2008.4543528.

[15] F. Petit, W. Friedl, H. Hoppner, and M. Grebenstein, "Analysis and synthesis of the bidirectional antagonistic variable stiffness mechanism," *IEEE/ASME Trans. Mechatronics*, vol. 20, no. 2, pp. 684–695, Apr. 2015, doi: 10.1109/TMECH.2014.2321428.

[16] J. W. Hurst, J. E. Chestnutt, and A. A. Rizzi, "The actuator with mechanically adjustable series compliance," *IEEE Trans. Robot.*, vol. 26, no. 4, pp. 597–606, Aug. 2010, doi: 10.1109/TRO.2010.2052398.

[17] C. E. English and D. Russell, "Mechanics and stiffness limitations of a variable stiffness actuator for use in prosthetic limbs," *Mech. Mach. Theory*, vol. 34, no. 1, pp. 7–25, Jan. 1999, doi: 10.1016/S0094-114X(98)00026-3.

[18] E. Hocaoglu and V. Patoglu, "Design, implementation and evaluation of a variable stiffness transradial hand prosthesis," 2019, *arXiv:1910.12569*. [Online]. Available: http://arxiv.org/abs/1910.12569

[19] R. Van Ham, B. Vanderborght, M. Van Damme, B. Verrelst, and D. Lefeber, "MACCEPA, the mechanically adjustable compliance and controllable equilibrium position actuator: Design and implementation in a biped robot," *Robot. Auton. Syst.*, vol. 55, no. 10, pp. 761–768, Oct. 2007, doi: 10.1016/j.robot.2007.03.001.

[20] B. Vanderborght, N. G. Tsagarakis, R. Van Ham, I. Thorson, and D. G. Caldwell, "MACCEPA 2.0: Compliant actuator used for energy efficient hopping robot Chobino1D," *Auton. Robots*, vol. 31, no. 1, pp. 55–65, Jul. 2011, doi: 10.1007/s10514-011-9230-7.

[21] S. Wolf, O. Eiberger, and G. Hirzinger, "The DLR FSJ: Energy based design of a variable stiffness joint," in *Proc. IEEE Int. Conf. Robot. Automat.*, May 2011, pp. 5082–5089, doi: 10.1109/ICRA.2011.5980303.

[22] V. Grosu, C. Rodriguez-Guerrero, S. Grosu, B. Vanderborght, and D. Lefeber, "Design of smart modular variable stiffness actuators for robotic-assistive devices," *IEEE/ASME Trans. Mechatronics*, vol. 22, no. 4, pp. 1777–1785, Aug. 2017, doi: 10.1109/TMECH.2017.2704665.

[23] B. Vanderborght *et al.*, "Variable impedance actuators: A review," *Robot. Auton. Syst.*, vol. 61, no. 12, pp. 1601–1614, Dec. 2013, doi: 10.1016/j.robot.2013.06.009.

[24] R. Ham, T. Sugar, B. Vanderborght, K. Hollander, and D. Lefeber, "Compliant actuator designs," *IEEE Robot. Autom. Mag.*, vol. 16, no. 3, pp. 81–94, Sep. 2009, doi: 10.1109/MRA.2009.933629.

[25] N. L. Tagliamonte, F. Sergi, D. Accoto, G. Carpino, and E. Guglielmelli, "Double actuation architectures for rendering variable impedance in compliant robots: A review," *Mechatronics*, vol. 22, no. 8, pp. 1187–1203, Dec. 2012, doi: 10.1016/j.mechatronics.2012.09.011.

[26] B. Vanderborght, R. Van Ham, D. Lefeber, T. G. Sugar, and K. W. Hollander, "Comparison of mechanical design and energy consumption of adaptable, passive-compliant actuators," *Int. J. Robot. Res.*, vol. 28, no. 1, pp. 90–103, Jan. 2009, doi: 10.1177/0278364908095333.

[27] V. Chalvet and D. J. Braun, "Criterion for the design of low-power variable stiffness mechanisms," *IEEE Trans. Robot.*, vol. 33, no. 4, pp. 1002–1010, Aug. 2017, doi: 10.1109/TRO.2017.2689068.

[28] T. Verstraten, P. Beckerle, R. Furnémont, G. Mathijssen, B. Vanderborght, and D. Lefeber, "Series and parallel elastic actuation: Impact of natural dynamics on power and energy consumption," *Mechanism Mach. Theory*, vol. 102, pp. 232–246, Aug. 2016, doi: 10.1016/j.mechmachtheory.2016.04.004.

[29] B. Vanderborght, B. Verrelst, R. Van Ham, M. Van Damme, D. Lefeber, B. M. Y. Duran, and P. Beyl, "Exploiting natural dynamics to reduce energy consumption by controlling the compliance of soft actuators," *Int. J. Robot. Res.*, vol. 25, no. 4, pp. 343–358, Apr. 2006, doi: 10.1177/0278364906064566.

[30] L. C. Visser, R. Carloni, and S. Stramigioli, "Energy-efficient variable stiffness actuators," *IEEE Trans. Robot.*, vol. 27, no. 5, pp. 865–875, Oct. 2011, doi: 10.1109/TRO.2011.2150430.

[31] L. Liu, S. Leonhardt, and B. J. E. Misgeld, "Design and control of a mechanical rotary variable impedance actuator," *Mechatronics*, vol. 39, pp. 226–236, Nov. 2016, doi: 10.1016/j.mechatronics.2016.06.002.

[32] B. J. E. Misgeld, L. Hewing, L. Liu, and S. Leonhardt, "Closed-loop positive real optimal control of variable stiffness actuators," *Control Eng. Pract.*, vol. 82, pp. 142–150, Jan. 2019, doi: 10.1016/j.conengprac.2018.08.022.

[33] B.-S. Kim and J.-B. Song, "Design and control of a variable stiffness actuator based on adjustable moment arm," *IEEE Trans. Robot.*, vol. 28, no. 5, pp. 1145–1151, Oct. 2012, doi: 10.1109/TRO.2012.2199649.

[34] J. Sun, Y. Zhang, C. Zhang, Z. Guo, and X. Xiao, "Mechanical design of a compact serial variable stiffness actuator (SVSA) based on lever mechanism," in *Proc. IEEE Int. Conf. Robot. Automat. (ICRA)*, May 2017, pp. 33–38, doi: 10.1109/ICRA.2017.7988687.

[35] W. Wang, Y. Zhao, and Y. Li, "Design and dynamic modeling of variable stiffness joint actuator based on archimedes spiral," *IEEE Access*, vol. 6, pp. 43798–43807, 2018, doi: 10.1109/ACCESS.2018.2864100.

[36] M. I. Awad, D. Gan, I. Hussain, A. Az-Zu'bi, C. Stefanini, K. Khalaf, Y. Zweiri, J. Dias, and L. D. Seneviratne, "Design of a novel passive binary-controlled variable stiffness joint (BpVSJ) towards passive haptic interface application," *IEEE Access*, vol. 6, pp. 63045–63057, 2018, doi: 10.1109/ACCESS.2018.2876802.

[37] D. S. Walker, D. J. Thoma, and G. Niemeyer, "Variable impedance magnetorheological clutch actuator and telerobotic implementation," in *Proc. IEEE/RSJ Int. Conf. Intell. Robots Syst.*, Oct. 2009, pp. 2885–2891, doi: 10.1109/IROS.2009.5354689.

[38] M. I. Awad, I. Hussain, D. Gan, A. Az-Zu'bi, C. Stefanini, K. Khalaf, Y. Zweiri, T. Taha, J. Dias, and L. Seneviratne, "Passive discrete variable stiffness joint (pDVSJ-II): Modeling, design, characterization, and testing toward passive haptic interface," *J. Mech. Robot.*, vol. 11, no. 1, pp. 1–14, Feb. 2019, doi: 10.1115/1.4041640.

[39] V.-D. Nguyen, "Constructing force-closure grasps," *Int. J. Robot. Res.*, vol. 7, no. 3, pp. 3–16, Jun. 1988, doi: 10.1177/027836498800700301.

[40] M. Erdmann, "On a representation of friction in configuration space," *Int. J. Robot. Res.*, vol. 13, no. 3, pp. 240–271, Jun. 1994, doi: 10.1177/027836499401300306.

[41] R. G. Budynas and J. K. Nisbett, *Shigley's Mechanical Engineering Design*, 9th ed. New York, NY, USA: McGraw-Hill, 2017.

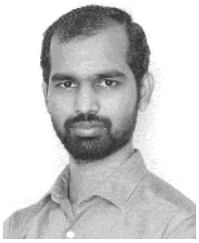

NAGAMANIKANDAN GOVINDAN received the B.E. degree in electronics and communication and the M.E. degree in mechatronics engineering from Anna University, India. He is currently pursuing the Ph.D. degree in robotics with the Department of Engineering Design, Indian Institute of Technology Madras, India. His research interests include multimodal robot design, control strategies, variable stiffness actuators, grasping, and manipulation.

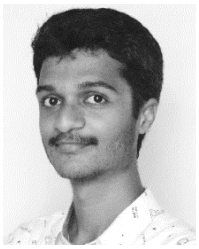

SHASHANK RAMESH is currently pursuing the B.Tech. degree in mechanical engineering with integrated Master's program in robotics with the Indian Institute of Technology Madras, India. His research interests are in the field of dynamics and control of robots.

ASOKAN THONDIYATH (Senior Member, IEEE) received the B.Tech. and M.Tech. degrees in mechanical engineering from Calicut University and the Ph.D. degree in mechanical engineering from the Indian Institute of Technology Madras, in 2000. He is currently a Professor with the Department of Engineering Design and the Head of the Department at IIT Madras, India. He spent six years as a Researcher at the Robotics Research Center, Nanyang Technological University, Singapore, working in the area of mechatronic systems and robotics. He was instrumental in developing the remotely operated underwater vehicle and a 7-axis underwater manipulator at NTU, Singapore. Prior to this, he spent three years in DRDO as a Scientist. He has published more than 130 papers in International journals and conferences and has filed 18 patents in India, USA, and Singapore. His areas of teaching and research are robotics, product design, and engineering system design. He was awarded the Stanford-India Biodesign fellowship by Stanford University, USA, in 2009, and has completed a post-doctoral fellowship in medical device development at Stanford University. He is currently the National Secretary of The Robotics Society, India.